Available online at www.sciencedirect.com
ScienceDirect
Polymer 48 (2007) 3452–3460
polymer
www.elsevier.com/locate/polymer

# Structure and crystallization behavior of Nylon 66/multi-walled carbon nanotube nanocomposites at low carbon nanotube contents

Lingyu Li [a], Christopher Y. Li [a,*], Chaoying Ni [b], Lixia Rong [c], Benjamin Hsiao [c]

[a] *A.J. Drexel Nanotechnology Institute and Department of Materials Science and Engineering, Drexel University, Philadelphia, PA 19104, United States*
[b] *W.M. Keck Electron Microscopy Facility, Department of Materials Science and Engineering, University of Delaware, Newark, DE 19716, United States*
[c] *Department of Chemistry, Stony Brook University, Stony Brook, NY 11794, United States*

Received 8 February 2007; received in revised form 5 April 2007; accepted 11 April 2007
Available online 21 April 2007

**Abstract**

Multi-walled carbon nanotubes (MWNTs) were modified with poly(hexamethylene adipamide) (also known as Nylon 66) via a controlled polymer solution crystallization method. A ''nanohybrid shish kebab'' (NHSK) structure was found wherein the MWNT resembled the shish while Nylon 66 lamellar crystals formed the kebabs. These Nylon 66-functionalized MWNTs were used as precursors to prepare polymer/MWNT nanocomposites. Excellent dispersion was revealed by optical and electron microscopies. Nitric acid etching of the nanocomposites showed that MWNT formed a robust network in Nylon 66. Non-isothermal DSC results showed multiple melting peaks, which can be attributed to lamellar thickness changes upon heating. The crystallite sizes $L_{100}$ and $L_{010}$ of Nylon 66, determined by WAXD, decreased with increasing MWNT contents. Isothermal DSC results showed that crystallization kinetics increased first and then decreased with increasing MWNT contents in Nylon 66. This study showed that the effect of MWNTs on Nylon 66 crystallization is twofold: MWNTs provide heterogeneous nucleation sites for Nylon 66 crystallization while the tube network structure hinders large crystal growth.


*Keywords:* Polymer nanocomposites; Carbon nanotube; Polymer crystallization

## 1. Introduction

Since their discovery, carbon nanotubes (CNTs) have attracted tremendous attention due to their unique properties such as high mechanical strength and high electrical conductivity [1,2]. One of the most promising applications of CNTs is polymer/CNT nanocomposites [1,3]. Combination of their superb physical properties with the high aspect ratio makes CNT an excellent reinforcing material for high-performance and multifunctional polymer nanocomposites [2,4]. Depending upon the targeted properties, a variety of polymers have been explored, including amorphous polymers such as polystyrene [5–7], poly(methyl methacrylate) [8–10], rigid rod polymers such as poly(*p*-phenylene benzobisoxazole) [11], crosslinkable polymers such as epoxy [12–14], conducting polymers such as polyaniline, polypyrrole [15–18], and crystalline polymers (see later). Due to the small diameter and extremely hydrophobic surface property of CNTs, however, it is difficult to achieve homogenous dispersion of CNTs within a polymeric material matrix. This dramatically hinders rapid progress in the field. In order to overcome these technical hurdles, it is desirable to modify the CNT surface with polymers that are either identical or structurally similar to matrix materials [2]. Among all the existing CNT surface modification methods, the noncovalent method is advantageous due to its non-destructive nature [19,20]. We recently reported a polymer crystallization method to modify CNT and nanofibers with semicrystalline polymers in a periodic manner, leading to a novel ''nanohybrid shish kebab'' (NHSK) nanostrucutre [4,21–23]. Compared with other noncovalent CNT

* Corresponding author. Tel.: +1 215 895 2083; fax: +1 215 895 6760.
*E-mail address:* chrisli@drexel.edu (C.Y. Li).

0032-3861/$ - see front matter © 2007 Elsevier Ltd. All rights reserved.
doi:10.1016/j.polymer.2007.04.030

functionalization methods such as surfactant [24,25] or amorphous polymer wrapping [26] previously reported by other groups, our technique has the following advantages: (1) crystalline polymers are mechanically more robust than small molecules and amorphous polymers; they are thus preferable for composite reinforcement; (2) the three-dimensional (3D) complex structure of NHSK makes it a better candidate for reinforcement due to the ''nanoanchor effect'' [27]; (3) a variety of functional groups can be introduced to the polymer chain ends. Upon crystallization, these functional groups will be excluded to the lamellar surface near the vicinity of CNTs, which enables CNT functionalization. This method has been employed to modify CNTs with polyethylene (PE); PE/CNT nanocomposites were synthesized. Excellent CNT dispersion and 70–90 °C thermal stability enhancement were observed at low CNT contents [4].

Polyamide (Nylon) is an important thermoplastic material with numerous applications. Reinforcing Nylon with CNTs has been recently investigated by a number of groups [28–33]. Chemical functionalization of MWNTs using the surface carboxylic acid groups has been used to surface-graft Nylon chains. Winey et al. reported the use of purified, chemical functionalized, and surfactant stabilized SWNTs for interfacial *in situ* polymerization with Nylon 66 [28]. It was revealed that only the chemical functionalized SWNT exhibited uniform dispersion of SWNTs whilst composites containing purified SWNTs exhibited poor dispersions in the composite. Though the chemical functionalized version exhibited better dispersion, the electrical conductivity test of the extruded composite rods showed that the purified Nylon 66/SWNT composite was more conductive compared to the chemical functionalized version of the composite.

In this article, we report functionalization of multi-wall CNTs (MWNTs) with Nylon 66 via polymer solution crystallization method to obtain Nylon 66/MWNT NHSK nanostructures. These NHSKs were then used as precursors to form Nylon 66/MWNT nanocomposites. Nanocomposites with MWNT contents from 0.1 to 2 wt% were fabricated. Structure, morphology and crystallization behavior of these nanocomposites were systematically characterized using transmission electron microscopy (TEM), scanning electron microscopy (SEM), polarized light microscopy (PLM), wide-angle X-ray diffraction (WAXD) and Raman spectroscopy. Non-isothermal and isothermal differential scanning calorimetric (DSC) experiments were conducted for crystallization behavior studies. Detailed crystallization behavior of Nylon 66/MWNT composites will be discussed.

## 2. Experimental section

### 2.1. Materials and sample preparation

MWNTs were purchased from Aldrich. The MWNTs were washed with 2.4 M nitric acid for 0.5 h and rinsed with methanol. The resulting MWNTs were then centrifuged, collected and dried in a vacuum oven. Nylon 66 ($Mn = 10{,}000$ g/mol) was supplied by DuPont Company. Nylon 66/MWNT NHSKs were obtained using a controlled solution crystallization method [34,35]. Glycerin was used as the solvent and the concentration was ~0.01 wt%. Nylon 66 was dissolved in glycerin at 240 °C. MWNT (0.1 mg) was dispersed in 1 g glycerin and ultrasonicated for 1–2 h at 40 °C and then added to a 9 g (w/w) 0.01% Nylon 66/glycerin solution at 240 °C. The mixture was then quenched to the preset $T_c$. The crystallization time was controlled to be 0.5–3 h. The system was purged with $N_2$ gas during the entire process. Samples were also isothermally filtered after crystallization to remove the uncrystallized polymers. Glycerin was exchanged with isopropanol at room temperature for TEM sample preparation. The preparation of the Nylon 66/MWNT nanocomposites was accomplished by adding extra Nylon 66/glycerol solution (~1–5 wt%) to the preformed NHSKs at $T_c$ and further crystallizing for 3 h. The system was then cooled to room temperature. Upon filtering to remove the glycerol, the grayish solid sample was washed thoroughly with isopropanol and was kept in vacuum oven overnight. Nylon 66/MWNT nanocomposites with controlled MWNT contents (0.1–2 wt%) were then obtained.

### 2.2. Characterization

TEM experiments were conducted using a JEOL-2000FX microscope with an accelerating voltage of 120 kV. SEM experiments were carried out using a FEI/Phillips XL30 field emission environmental SEM and the acceleration voltage was 15 kV. WAXD experiments were performed at Brookhaven National Laboratory's national synchrotron light source using the beamline X27C. The wavelength ($\lambda$) of the X-ray beam was 0.1307 nm. Raman spectra were acquired with a Raman microspectrometer (Renishaw 1000) using a diode laser (780 nm) in back-scattering geometry. A 50× objective was used with a spot size of ~1 μm in diameter, which included a large area of samples, providing statistically reliable results. The laser power was kept low to avoid overheating of the samples. DSC experiments were performed using a Perkin–Elmer DSC-7. The samples were heated first, then cooled and heated again at the same scanning rate (10 °C/min) under a nitrogen atmosphere in order to avoid oxidation. Samples with a typical mass of 3–5 mg were encapsulated in sealed aluminum pans. The temperature and heat flow were calibrated using standard materials at different cooling and heating rates between 5 and 40 °C/min. A PLM (Olympus BX-51) coupled with Mettler hot stage (FP 82 HT with a FP-90 central processor) was used to characterize MWNT dispersion. The image was captured using an Insight digital camera. The nanocomposite film was prepared by the melt-pressing method.

## 3. Results and discussion

### 3.1. Nylon 66 modified MWNTs

Fig. 1a shows an SEM image of Nylon 66 decorated MWNTs which was obtained by crystallizing Nylon 66 in

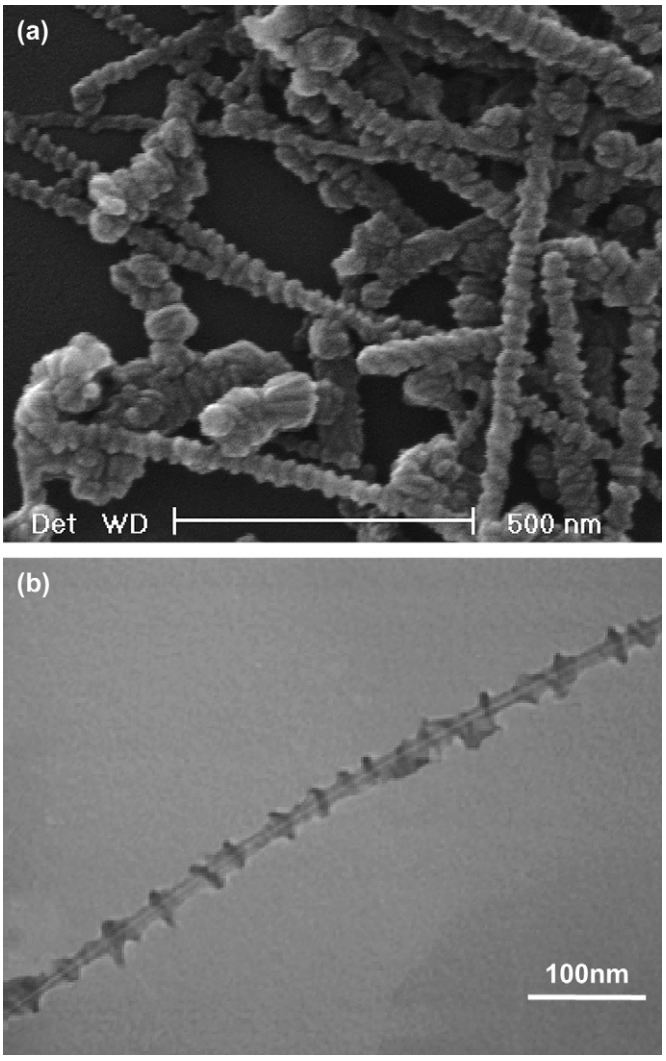


Fig. 1. (a) SEM image of Nylon 66-functionalized MWNT; (b) TEM image of the similar structure.

MWNT/glycerin suspension at 185 °C for 0.5 h. It is evident that MWNTs formed the central stems and disc-shaped objects periodically decorated the MWNT surface. All the MWNTs were separated as individual tubes. The disc-shaped objects are edge-on views of the Nylon 66 single crystal lamellae and the morphology is similar to the classical polymer shish kebab structures formed in an elongation/shear flow field [36]. The MWNT/polymer solution in this case was not under external flow during crystallization and it is the MWNT that induces nucleation of Nylon 66 molecules upon the MWNT surface. This unique nanohybrid structure in Fig. 1 was thus named NHSK [21–23]. Note that the lamellae appear to be "thick" in the figure since they were sputtered with Pt. Fig. 1b shows a TEM micrograph of a similar structure without Pt shadowing. The lateral dimension of the kebab is ~20 nm in Fig. 1b and the periodicity is ~20–30 nm. The lamellae decorated on the MWNTs thus serve as ideal "spacers" which prohibited MWNTs from agglomeration. These images show convincingly that MWNTs can initiate Nylon 66 crystallization.

### *3.2. Nylon 66/MWNT nanocomposites, crystal morphology and structure*

The NHSK formation process evidenced the ability to facilitate the CNT dispersion in organic solvents and was thus used for nanocomposites' fabrication. Since the kebabs are lamellar crystals formed in solution, the lateral size of these lamellae could be easily controlled by tuning the crystallization conditions such as crystallization temperature ($T_c$) and time ($t$). Fig. 2 shows an SEM image of Nylon 66 crystallized on MWNTs (arrows) in glycerin at 180 °C for 0.5 h. Much larger kebabs could be clearly seen and these lamellae closely follow the geometry of MWNTs. Due to the large size, the lamellar crystals do not show clear orientation as opposed to the regular hybrid structure in Fig. 1.

In order to prepare Nylon 66/MWNT nanocomposites, extra Nylon 66/glycerol solution (~1–5 wt%) was added to the preformed NHSK suspension at $T_c$ (185 °C) and was allowed to further crystallize for 3 h. The mixture was then cooled to room temperature. The results and schematic representation of the preparation process are shown in Fig. 3. As the SEM images in Fig. 3 show, Nylon 66 forms rounded spherulites and the average diameter of the hybrid spherulites is about 10 μm. Nylon 66 lamellae can be clearly seen. Note that these two images also represent the conventional neat Nylon 66 negative spherulites formed at high $T_c$. From these two figures, one cannot tell whether MWNTs were embedded in the Nylon 66 spherulites. Etching these spherulites with nitric acid, however, reveals the hybrid nature of the spherulites as shown in Fig. 4a and b. Adding one drop of nitric acid on a Nylon 66 hybrid spherulites containing 0.5 wt% MWNT and etching for 20 min resulted in partially etched Nylon 66 spherulites, since amorphous regions of the spherulites were first removed. One intriguing observation from Fig. 4a and b is that, MWNT networks are clearly seen in the hole areas formed by nitric acid etching. The MWNTs are relatively large in diameter,

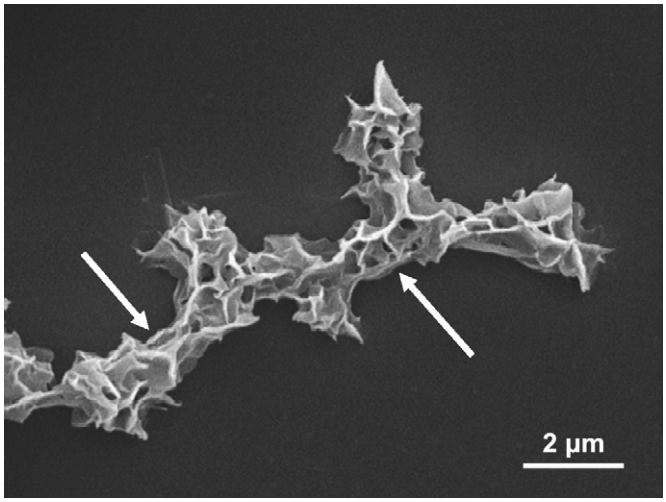


Fig. 2. Nylon 66-wrapped MWNT structure produced by crystallization of Nylon 66 on MWNTs at 180 °C in glycerin for 0.5 h. The SEM image shows that MWNTs are wrapped with Nylon 66 crystals.

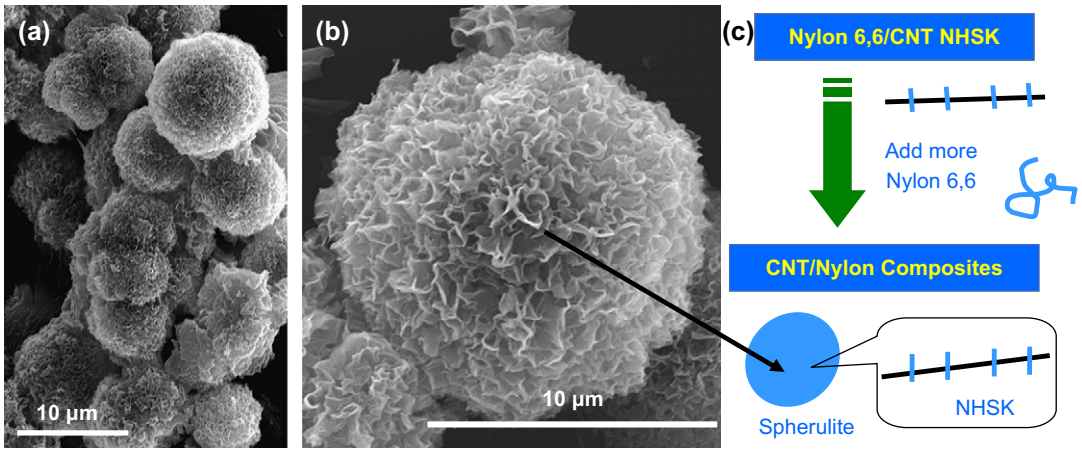


Fig. 3. (a) and (b) are the SEM micrographs at different magnifications of 0.5 wt% CNT/Nylon 66 nanocomposites (negative Nylon 66 spherulites) formed by using NHSK as seeds to further crystallize Nylon 66 at 185 °C; (c) schematic of the preparation of nanocomposites.

which is perhaps due to the surface coating of a layer of Nylon 66. NHSK structures can be occasionally seen from the holes (arrows), indicating good interfacial adhesion of Nylon 66 crystals to MWNT surface. Since the negative Nylon 66 spherulites were formed using the NHSK shown in Fig. 1b as the precursors, observation of the NHSK network within a Nylon 66 spherulite indicates that, upon forming NHSK at 185 °C, the network structure of NHSK in glycerin is relatively robust. As Nylon 66 spherulites grew, the diffusion and growth of Nylon 66 failed to repel the adjacent NHSK; instead, the spherulite engulfed the NHSKs, which led to the observation of negative Nylon 66 spherulites with closely packed NHSK network inside. These composites were melt-pressed to form polymer films which were subjected to PLM observation. As Fig. 4c and d shows, at $T_c \sim 180$ °C, neat Nylon 66 crystallized into large spherulites whilst nanocomposites formed a texture with a fine grain size upon crystallization, due to the nanoconfinement/multiple nucleation effects of MWNTs.

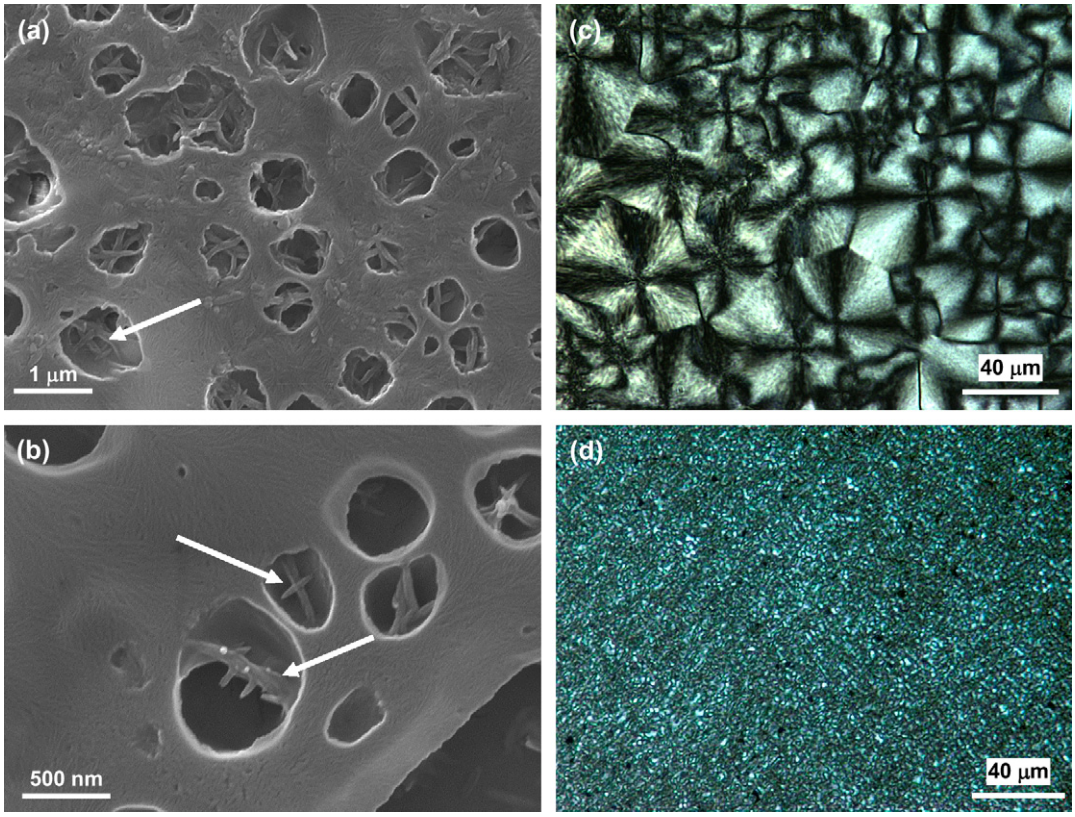


Fig. 4. (a) SEM image of 0.5 wt% Nylon 66/MWNT nanocomposites after nitric acid etching for 20 min; (b) shows higher magnification SEM images of NHSK found in the hole areas of the etched Nylon 66/MWNT spherulites. (c) and (d) are PLM images of Nylon 66 and 0.5 wt% Nylon 66/MWNT nanocomposite films. The films were prepared by the melt-pressing method.

Similar effects have also been observed in polymer nanoclay nanocomposites [37]. The 0.5 wt% MWNT/Nylon 66 nanocomposite film also showed a homogenous distribution of MWNT on a micrometer scale as revealed by the PLM image in Fig. 4d.

MWNT contents of the nanocomposites were semi-quantitatively evaluated using Raman spectroscopy. Fig. 5 shows the spectra of MWNT, Nylon 66 and the nanocomposites. G band at 1580 $cm^{-1}$ does not overlap with any bands in the Nylon 66 Raman spectrum and therefore can be used as the reference to semi-quantitatively compare the MWNT composition in the nanocomposites. The band at 1636 $cm^{-1}$ is due to C=O stretch of amide groups in Nylon 66 [38]. As the loading of MWNT increased, the ratio of these two bands also increased; at 2 wt% MWNT loading, the intensity of G band became much higher than amide group band.

The crystalline structure of MWNT/Nylon 66 nanocomposites was characterized using the WAXD technique. WAXD patterns are displayed in Fig. 6. Two distinct peaks observed at $2\theta$ of 18.11° and 21.04° is consistent with diffraction of (100) and (010,110) crystalline planes, respectively [39]. These two diffraction peaks indicate that Nylon 66 crystallized in the triclinic $\alpha$ form. The crystallite size perpendicular to the diffraction ($hkl$) plane, $L_{hkl}$ in nanometers, can be obtained by using the Scherrer expression [40]:

$$L_{hkl} = \frac{k\lambda}{\beta \cos\theta}$$

where $\beta = (B^2 - b_0^2)^{1/2}$ is pure line breadth, $B$ is a measured half-width of the experimental peak (in degrees). $b_0$ is the instrumental broadening factor which is approximately equal to 0.15°. $K$ is the Scherrer factor, which is ~0.9 if the Gaussian equation is employed. $\lambda$ is the X-ray wavelength and $2\theta$ is the Bragg angle. The crystallite sizes calculated are listed in Table 1. The crystallite sizes $L_{(100)}$ and $L_{(010)/(110)}$ of Nylon 66 slightly decreased with an increasing MWNT content, which can be attributed to the nanoconfinement effects of the CNT network.

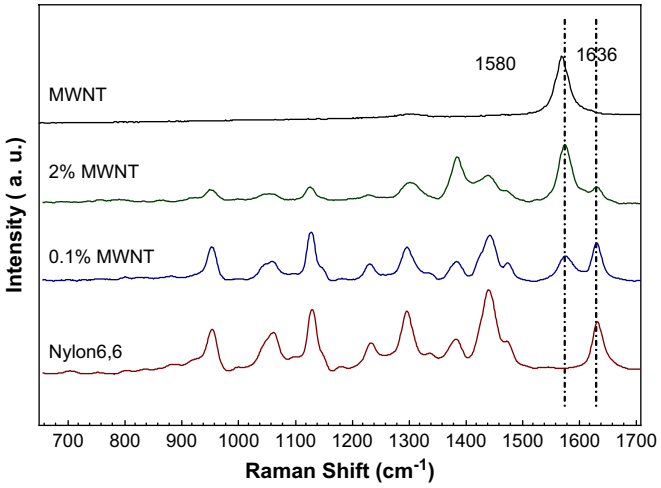


Fig. 5. Raman spectra of Nylon 66 and Nylon 66/MWNT nanocomposites.

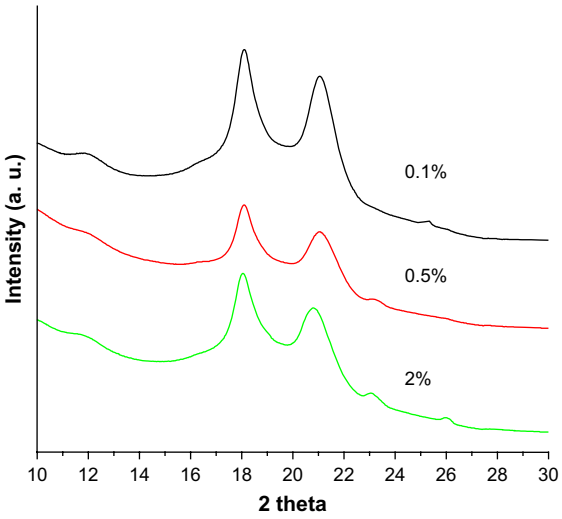


Fig. 6. Wide-angle X-ray diffraction patterns of Nylon 66/MWNT nanocomposites.

Table 1
Crystallite size of Nylon 66/MWNT nanocomposites

| MWNT content (wt%) | $L_{100}$ (nm) | $L_{010}$ (nm) |
|---|---|---|
| 0.1 | 4.15 | 4.39 |
| 0.5 | 4.04 | 4.25 |
| 2 | 3.83 | 4.06 |

### 3.3. Nylon 66/MWNT nanocomposites, crystallization behavior

DSC was employed to evaluate the effect of MWNTs on the phase transition behavior of Nylon 66. Fig. 7 shows DSC 1st cooling and 2nd heating thermograms obtained at 10 °C/min rate. The crystallization temperature, $T_c$, obtained from the minimum of exothermic peak is about 228 °C for Nylon 66. The addition of 0.1–2 wt% MWNTs into Nylon 66 led to a shift of crystallization peak mainly towards lower $T_c$ while the onset temperatures remained similar ($T_{on\text{-}Nylon\ 66} = 231$ °C, $T_{on\text{-}0.1\%} = 232$ °C, $T_{on\text{-}0.5\%} = 228$ °C and $T_{on\text{-}2\%} = 232$ °C). This observation is intriguing since Fig. 1 shows that MWNT can initiate Nylon 66 crystallization, and one expect a similar, if not higher $T_c$ for the composite samples. This contradictory can be explained by the nanoconfinement/multiple nucleation effects: similar onset temperatures indicate that non-isothermal crystallization of Nylon 66 and nanocomposites started at similar temperatures, however, MWNT network imposed a confinement effect on polymer chain diffusion and crystal growth. This confinement slowed down crystallization process, which led to lower $T_c$s for nanocomposites. Note that the surface chemistry of MWNT could also affect polymer crystallization as previously discussed [23].

DSC heating curves in Fig. 7 show two melting peaks at 245.5 °C ($T_{m1}$) and 259 °C ($T_{m2}$). The addition of MWNTs did not change $T_{m1}$. However, with increasing MWNT contents, $T_{m2}$ shifted to lower temperature and the heat of fusion of the $T_{m1}$ increased and that of $T_{m2}$ decreased. The behavior

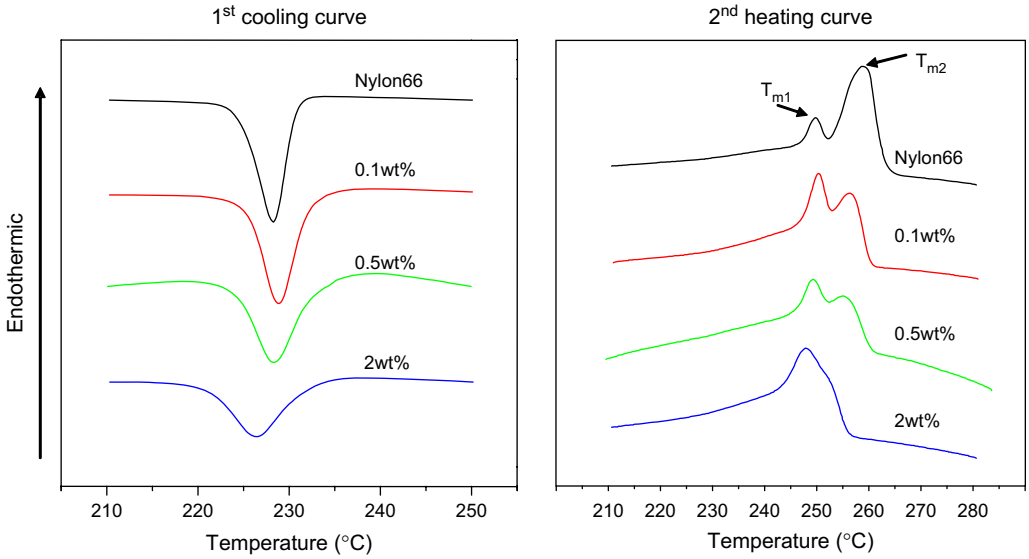


Fig. 7. Non-isothermal DSC scans of Nylon 66/MWNT nanocomposites. Heating and cooling rates are 10 °C/min. $T_{m1}$ and $T_{m2}$ are marked with arrows.

of multi-melting peaks in Nylon 66 has been observed and discussed before for both pristine Nylon 66 [41,42] and Nylon 66 nanocomposites [43–46]. Bell et al. reported that Nylon 66 exhibited two melting peaks, which might appear singly or together depending on the annealing and drawing treatment [41]. They suggested that there were two distinct morphological species: form I and form II, where form II was thermodynamically preferred while form I was kinetically preferred. They also noted that these two forms were not related to the α and β structures proposed by Bunn and Garner [47]. Khoury has elegantly demonstrated that negative Nylon 66 spherulites melted at higher temperature than the

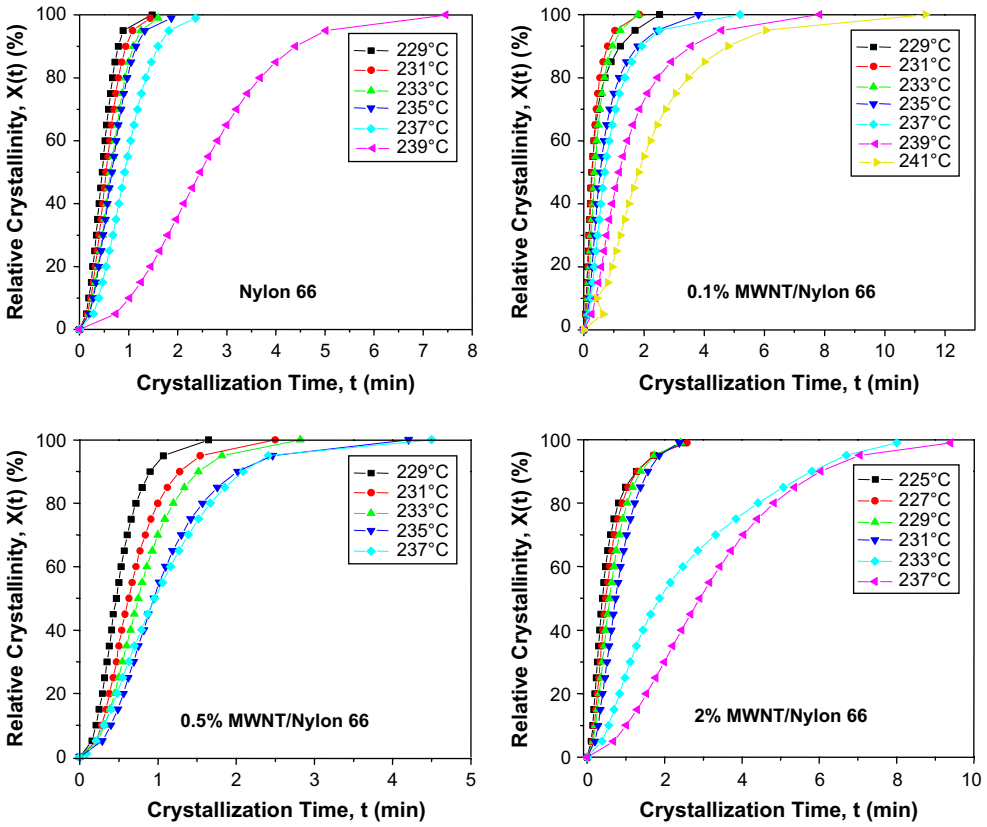


Fig. 8. Relative crystallinity $X(t)$ versus different crystallization time $t$ in the process of isothermal crystallization for pure Nylon 66 and Nylon 66/MWNT nanocomposites.

positive ones [48]. In the DSC run, it was pointed out later that the multiple melting peaks were probably due to rearrangement of the lamellae since Nylon 66 crystals could easily thicken upon annealing [42,49]. $T_{m1}$ is generally attributed to the thin lamellae formed during cooling and $T_{m2}$ is attributed to the melting of the thickened crystals during the heating/annealing process. In the present case, the heat of fusion of the two melting peaks in Nylon 66 and nanocomposites varied following such a trend that as MWNT content increased, the heat of fusion of peak one increased while that of peak two decreased. This change could be attributed to the fact that as the MWNT contents increased, the MWNT network formed in the Nylon 66 spherulites dramatically slowed down the lamellar thickening process and less crystals were thickened, leading to a higher heat of fusion of the $T_{m1}$ peak in the nanocomposites as opposed to the neat Nylon 66 case. A similar phenomenon was reported in Nylon 66/nanoclay systems [45,50,51].

Isothermal crystallization behavior of Nylon 66/MWNT nanocomposites was also studied using DSC and the results are shown in Figs. 8 and 9. The relative degree of crystallinity at time $t$, $X(t)$, is defined as the following:

$$X(t) = \frac{X_c(t)}{X_c(t_\infty)} = \frac{\int_0^t \frac{dH(t)}{dt}\,dt}{\int_0^{t\infty} \frac{dH(t)}{dt}\,dt} = \frac{\Delta H_t}{\Delta H_\infty}$$

where $dH/dt$ is the rate of heat evolution; $\Delta H_t$ is the heat generated at time $t$; $\Delta H_\infty$ is the total heat by the end of the crystallization process. Fig. 8 shows the relative crystallinity at different crystallization times in the process of isothermal crystallization. It can be seen that the characteristic sigmoid isotherms shift to the right with increasing $T_c$ and the crystallization rate becomes slower. The Avrami equation [52] was used to analyze the crystallization process as the following:

$$X(t) = 1 - \exp(-Kt^n)$$

$$\lg(-\ln(1 - X(t))) = n \lg t + \lg K$$

where $X(t)$ is the weight fraction of crystallized material at time $t$ (relative crystallinity); $n$ is the Avrami exponent and

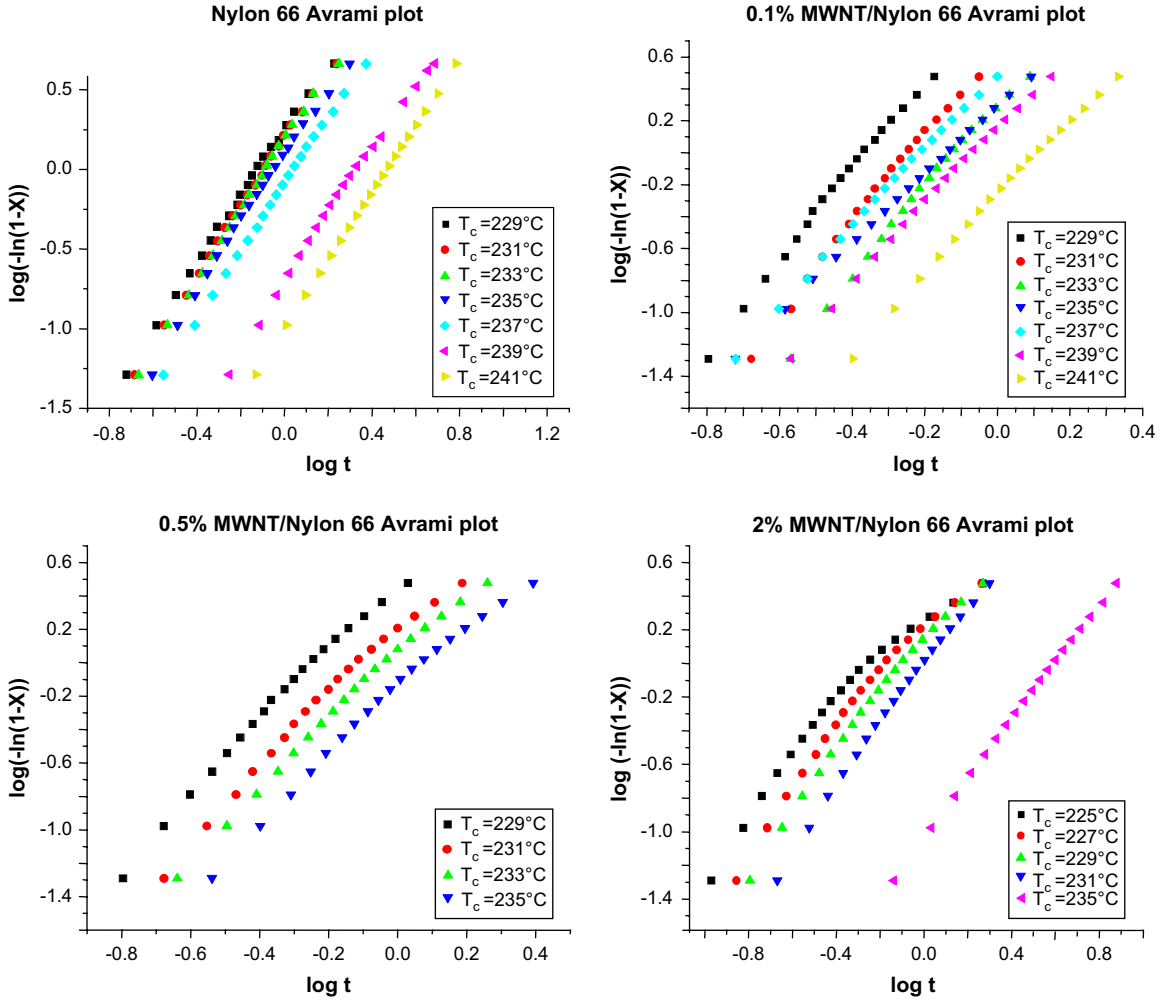


Fig. 9. Avrami plot for isothermal crystallization of Nylon 66 and Nylon 66/MWNT nanocomposite at the indicated temperatures.

$K$ is the crystallization rate parameter. The values of $n$ and $K$ are determined from the initial linear section of the figure and the results are shown in Tables 2–5.

It can be seen that the Avrami parameter $n$ varies from 1.65 to 2.15, depending on MWNT loading and temperature. These results indicate that spherulites' growth does not completely follow the spherulitic propagation (3D) [53]. In general, $n$ decreases slightly with adding MWNTs. Winey et al. reported similar observation in the PE/CNT nanocomposites [54]. Decreasing $n$ indicates that the growth dimension decreases as adding MWNTs, which can be attributed to two factors: (1) MWNTs serve as the 1D templates (nuclei) from polymer crystal growth, so that the initial consumption of the polymer melt is 1D in nature. (2) Due to the dense nucleation on the MWNT surfaces, the growth of the polymer crystals is confined between the adjacent crystals and the dimension is thus decreased.

The values of the crystallization rate parameters $K$ increased with decreasing crystallization temperature. At the same $T_c$, $K$ first increased as MWNT content reached 0.1 wt% and then decreased with an increasing MWNT content in Nylon 66. The effect of MWNT contents on crystallization rate parameter $K$ is plotted in Fig. 10, showing that the crystallization rate increased first and then decreased as MWNT content increased. This is consistent with the crystallization half-time $t_{1/2}$ observation. $t_{1/2}$ is defined as the time taken from the onset of the crystallization until 50% completion of the crystallization process and it can be extracted directly from the plot of $X(t)$ versus $t$ (Fig. 8). The results of $t_{1/2}$ are listed in Tables 2–5. It is evident that $t_{1/2}$ increased with increasing $T_c$. With increasing MWNT contents, $t_{1/2}$ first decreased and then increased. This, together with the non-isothermal DSC results previously discussed, suggests that the effect of MWNTs on Nylon 66 crystallization is twofold:

Table 2
Kinetic parameter for isothermal crystallization of Nylon 66

| $T_c$ (°C) | $n$ | $K$ (min$^{-n}$) | $t_{0.05}$ (min) | $t_{1/2}$ (min) |
|---|---|---|---|---|
| 229 | 2.19 | 3.85 | 0.14 | 0.46 |
| 231 | 2.12 | 2.51 | 0.16 | 0.54 |
| 233 | 2.15 | 1.84 | 0.19 | 0.63 |
| 235 | 2.10 | 1.63 | 0.2 | 0.66 |
| 237 | 2.15 | 0.82 | 0.28 | 0.92 |
| 239 | 2.16 | 0.20 | 0.56 | 1.74 |
| 241 | 2.12 | 0.10 | 0.74 | 2.46 |

Table 3
Kinetic parameters for isothermal crystallization of 0.1 wt% Nylon 66/MWNT nanocomposites

| $T_c$ (°C) | $n$ | $K$ (min$^{-n}$) | $t_{0.05}$ (min) | $t_{1/2}$ (min) |
|---|---|---|---|---|
| 229 | 1.65 | 5.94 | 0.06 | 0.27 |
| 231 | 1.74 | 5.96 | 0.07 | 0.28 |
| 233 | 1.75 | 3.77 | 0.11 | 0.37 |
| 235 | 1.72 | 1.92 | 0.13 | 0.55 |
| 237 | 1.72 | 1.25 | 0.17 | 0.70 |
| 239 | 1.69 | 0.52 | 0.27 | 1.18 |
| 241 | 1.77 | 0.24 | 0.44 | 1.82 |

Table 4
Kinetic parameters for isothermal crystallization of 0.5 wt% Nylon 66/MWNT nanocomposites

| $T_c$ (°C) | $n$ | $K$ (min$^{-n}$) | $t_{0.05}$ (min) | $t_{1/2}$ (min) |
|---|---|---|---|---|
| 229 | 2.15 | 3.23 | 0.16 | 0.47 |
| 231 | 2.06 | 1.62 | 0.21 | 0.63 |
| 233 | 2.00 | 1.12 | 0.23 | 0.75 |
| 235 | 1.91 | 0.69 | 0.29 | 0.95 |
| 237 | 1.69 | 0.70 | 0.31 | 0.96 |

Table 5
Kinetic parameters for isothermal crystallization of 2 wt% Nylon 66/MWNT nanocomposites

| $T_c$ (°C) | $n$ | $K$ (min$^{-n}$) | $t_{0.05}$ (min) | $t_{1/2}$ (min) |
|---|---|---|---|---|
| 225 | 1.84 | 4.06 | 0.10 | 0.39 |
| 227 | 1.89 | 2.75 | 0.13 | 0.48 |
| 229 | 1.78 | 1.74 | 0.16 | 0.58 |
| 231 | 1.78 | 1.12 | 0.22 | 0.73 |
| 233 | 1.68 | 0.29 | 0.38 | 1.87 |
| 237 | 1.74 | 0.11 | 0.68 | 2.91 |

MWNTs provide heterogeneous nucleation sites for Nylon 66 crystallization while the tube network structure hinders the formation of large-size crystals. At low MWNT contents, MWNT surface initiated Nylon crystallization and the nanoconfinement effect was not significant. As MWNT contents increase, although more MWNTs provided more nucleation surface, the formation of robust MWNT network imposed a much more significant nanoconfinement effect on Nylon 66 chains. This confinement effect overweighed the nucleation effect and slowed down the overall crystallization kinetics. Furthermore, we attempted to study if the nanoconfinement affects Nylon 66 crystallization at the early stage of the crystallization process by comparing $t_{0.05}$ with $t_{1/2}$. $t_{0.05}$ is defined as the time for achieving 5% relatively crystallinity. It represents the early stage crystallization behavior. From Tables 2–5, it is evident that the trend of $t_{0.05}$ is similar to that of $t_{1/2}$, indicating that the effect of MWNT on Nylon 66

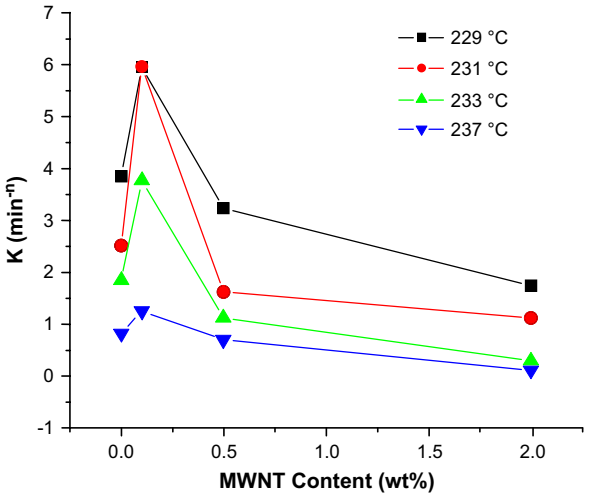


Fig. 10. Plot of the effect of MWNT contents on the crystallization rate parameter $K$.

crystallization (nucleation and nanoconfinement) is similar at the early and mid-stage of the crystallization. This is consistent with the non-isothermal crystallization results which showed decreased $T_c$ upon increasing MWNTs.

## 4. Conclusions

Noncovalent functionalization of MWNT with Nylon 66 single crystals was accomplished via controlled solution crystallization. Morphological study showed that the functionalized MWNT is similar to the classical shish kebab and the hybrid structure was named as nanohybrid shish kebabs. Nanocomposites were prepared using the Nylon 66 NHSKs as the precursors. Negative birefringent spherulites of Nylon 66 and MWNTs were obtained. Nitric acid etching revealed that MWNTs formed 3D networks in these Nylon 66 spherulites. The crystallite sizes $L_{100}$ and $L_{010}$ of Nylon 66, determined by WAXD, decreased with increasing MWNT contents. The effect of MWNT on Nylon 66 melting and crystallization behaviors was also examined. Multi-melting peaks were detected in the DSC experiments and were attributed to different lamellar thicknesses. As MWNT contents increased, heat of fusion of the lower temperature, endothermic peaking increased, suggesting that MWNT network might significantly hinder the lamellar thickening process. Isothermal crystallization showed that adding MWNTs in Nylon 66 slightly decreased its growth dimension. The crystallization rate increased first and then decreased with increasing MWNT contents.

## Acknowledgements

This work was supported by the NSF CAREER award (DMR-0239415), NSF DMI-0508407, 3M and DuPont. The WAXD experiments were carried out at the National Synchrotron Light Source at Brookhaven National Laboratory supported by the Department of Energy. Supply of Nylon 66 samples from DuPont (Dr. Mimi Keating) is appreciated.

## References

[1] Baughman RH, Zakhidov AA, de Heer WA. Science 2002;297:787.
[2] Thostenson ET, Ren ZF, Chou TW. Compos Sci Technol 2001;61:1899.
[3] Moniruzzaman M, Winey KI. Macromolecules 2006;39:5194.
[4] Kodjie SL, Li L, Li B, Cai WW, Li CY, Keating M. J Macromol Sci Phys 2006;45:231.
[5] Besancon BM, Green PF. Macromolecules 2005;38:110.
[6] Sabba Y, Thomas EL. Macromolecules 2004;37:4815.
[7] Hill DE, Lin Y, Rao AM, Allard LF, Sun YP. Macromolecules 2002; 35:9466.
[8] Kashiwagi T, Du FM, Winey KI, Groth KA, Shields JR, Bellayer SP, et al. Polymer 2005;46:471.
[9] Krishnan A, Dujardin E, Ebbesen TW, Yianilos PN, Treacy MMJ. Phys Rev B 1998;58:14013.
[10] Haggenmueller R, Gommans HH, Rinzler AG, Fischer JE, Winey KI. Chem Phys Lett 2000;330:219.
[11] Kumar S, Dang TD, Arnold FE, Bhattacharyya AR, Min BG, Zhang XF, et al. Macromolecules 2002;35:9039.
[12] Pecastaings G, Delhaes P, Derre A, Saadaoui H, Carmona F, Cui S. J Nanosci Nanotechnol 2004;4:838.
[13] Eitan A, Jiang KY, Dukes D, Andrews R, Schadler LS. Chem Mater 2003;15:3198.
[14] Thess A, Lee R, Nikolaev P, Dai HJ, Petit P, Robert J, et al. Science 1996;273:483.
[15] Chen GZ, Shaffer MSP, Coleby D, Dixon G, Zhou WZ, Fray DJ, et al. Adv Mater 2000;12:522.
[16] Chen J, Liu HY, Weimer WA, Halls MD, Waldeck DH, Walker GC. J Am Chem Soc 2002;124:9034.
[17] Zhang XT, Zhang J, Wang RM, Liu ZF. Carbon 2004;42:1455.
[18] Zhang XT, Zhang J, Wang RM, Zhu T, Liu ZF. Chemphyschem 2004;5:998.
[19] Hirsch A. Angew Chem Int Ed 2002;41:1853.
[20] Star A, Liu Y, Grant K, Ridvan L, Stoddart JF, Steuerman DW, et al. Macromolecules 2003;36:553.
[21] Li CY, Li L, Cai W, Kodjie SL, Tenneti KK. Adv Mater 2005;17:1198.
[22] Li L, Li CY, Ni C. J Am Chem Soc 2006;128:1692.
[23] Li L, Yang Y, Yang GL, Chen XM, Hsiao BS, Chu B, et al. Nano Lett 2006;6:1007.
[24] Chen J, Hamon MA, Hu H, Chen YS, Rao AM, Eklund PC, et al. Science 1998;282:95.
[25] Wang H, Zhou W, Ho DL, Winey KI, Fischer JE, Glinka CJ, et al. Nano Lett 2004;4:1789.
[26] O'Connell MJ, Boul P, Ericson LM, Huffman C, Wang YH, Haroz E, et al. Chem Phys Lett 2001;342:265.
[27] Bessho T, Inoue K, Kotwa I, Homma H. Electrochemistry 2006;74:299.
[28] Haggenmueller R, Du FM, Fischer JE, Winey KI. Polymer 2006; 47:2381.
[29] Zeng HL, Gao C, Wang YP, Watts PCP, Kong H, Cui XW, et al. Polymer 2006;47:113.
[30] Liu TX, Phang IY, Shen L, Chow SY, Zhang WD. Macromolecules 2004;37:7214.
[31] Sandler JKW, Pegel S, Cadek M, Gojny F, van Es M, Lohmar J, et al. Polymer 2004;45:2001.
[32] Qu LW, Veca LM, Lin Y, Kitaygorodskiy A, Chen BL, McCall AM, et al. Macromolecules 2005;38:10328.
[33] Kang M, Myung SJ, Jin HJ. Polymer 2006;47:3961.
[34] Geil PH. J Polym Sci 1960;44:449.
[35] Cai W, Li CY, Li L, Lotz B, Keating M, Marks D. Adv Mater 2004;16:600.
[36] Pennnings AJ, Kiel AM. Kolloid Z Z Polym 1965;205:160.
[37] Dillon DR, Tenneti KK, Li CY, Ko FK, Sics I, Hsiao BS. Polymer 2006;47:1678.
[38] Maddams WF, Royaud IAM. Spectrochim Acta Part A 1991;47:1327.
[39] Ramesh C, Keller A, Eltink S. Polymer 1994;35:2483.
[40] Alexander LE. X-ray diffraction methods in polymer science. New York: Wiley; 1969.
[41] Bell JP, Slade PE, Dumbleton JE. J Polym Sci Part A-2 1968;6:1773.
[42] Mitomo H, Nakazato K, Kuriyama I. Polymer 1978;19:1427.
[43] Weng WG, Chen GH, Wu DJ. Polymer 2003;44:8119.
[44] Liu MY, Zhao QX, Wang Y, Zhang CG, Mo ZS, Cao SK. Polymer 2003;44:2537.
[45] Zhang GS, Yan DY. J Appl Polym Sci 2003;88:2181.
[46] Li YJ, Zhu XY, Tian GH, Yan DY, Zhou EL. Polym Int 2001;50:677.
[47] Bunn C, Garner E. Proc R Soc London 1947;A-189:39.
[48] Khoury F. J Polym Sci 1958;33:389.
[49] Dreyfuss P, Keller A. J Polym Sci Part B 1970;8:253.
[50] Phang IY, Pramoda KP, Liu TX, He CB. Polym Int 2004;53:1282.
[51] Zhang QX, Yu ZZ, Yang MS, Ma J, Mai YW. J Polym Sci Part B Polym Phys 2003;41:2861.
[52] Avarami M. J Chem Phys 1939;7:1103.
[53] Wunderlich B. Macromolecular physics. New York: Academic Press; 1973.
[54] Haggenmueller R, Fischer JE, Winey KI. Macromolecules 2006;39:2964.